APPLICATION OF GNSS LENGTH METROLOGY TO CERN GEODETIC NETWORK

L. García-Asenjo, S. Baselga*, P. Garrigues, R. Luján, UPV, València, Spain
D. Pesce, IGN, Saint-Mandé, France
B. Weyer, J.F. Fuchs, D. Missiaen, CERN, Geneva, Switzerland

Abstract

Length determination in the open field is routinely done with electronic distance meters (EDMs) that are limited in accuracy by the imperfect knowledge of the index of refraction of the light path through the atmosphere so that obtaining distances of several kilometers within an accuracy of 10^{-7} is a major challenge. Refractivity compensated EDMs, from the initial designs of the early 1970s (e.g. the two-color Terrameter) until the last prototypes (e.g. the Arpent and the TeleYAG by CNAM and PTB, respectively) are exclusive solutions to overcome this problem which are not commercially available. By contrast, Global Navigation Satellite System (GNSS) technologies are relatively inexpensive positioning solutions that have experienced a wide adoption in the last decades. The use of scientific or commercial software for GNSS processing meets well the requirements of geodetic, surveying, and engineering applications but fails to do so in the field of length metrology, where the accurate uncertainty budget for all contributing error sources must be provided along with the resulting distance. We present our approach to GNSS-based length metrology, where all relevant error sources are characterized along with their uncertainties at the zero differences level in a relatively straightforward way and then rigorously propagated through the particular double-differenced equations used to obtain the distance. The method is applied to the CERN geodetic network using data from a GNSS campaign in July 2022 and the results are compared with those obtained for the same epoch by means of the Kern Mekometer ME5000 EDM as well as with other data available from previous campaigns.

INTRODUCTION

Length metrology is concerned with the realization, maintenance and dissemination of the SI meter. In the open air, the determination of distances consistent with the SI meter definition at a level of accuracy of the order of 10^{-7} is a challege at present. High precision Electronic Distance Meters (EDMs) may be used for this purpose, although the achievable accuracy is limited by the determination of the index of refraction along the light path with a degree of uncertainty of the same order, certainly a hard task because it entails the accurate determination of atmospheric parameters representative to the entire light path.

Refractivity compensated EDMs, from the early instruments developed in the late 1970s, e.g. the Terrameter [1], to the most recent telemeters, e.g. the 'Arpent' Absolute Distance Meter (ADM) and TeleYAG prototypes developed for the GeoMetre project [2], may serve for the purpose but, certainly, they are costly and not easily accessible solutions.

A possible alternative may be the use of Global Navigation Satellite Systems (GNSS) techniques. The GNSS scale is consistent with the SI meter definition by its maintenance by means of the use of atomic clocks and has been demonstrated to be worldwide stable at the level of 0.001 ppm (1 ppb). The use of GNSS for length metrology has been limited, however, due to the impossibility in the rigorous assessment of the contributing error sources and their corresponding uncertainties. This alternative was studied by a consortium of European metrology institutes and universities in the *Joint Research Project (JRP) SIB60 Metrology for long distance surveying* [3]. Their conclusions, summarized in their *Good practice guide for high accuracy global navigation satellite system based distance metrology* [4], indicate that the uncertainties of ionospheric and tropospheric delays, multipath effect and antenna phase center variations are mostly unknown, as is their propagation to the final results, which prevents a rigorous uncertainty analysis of the GNSS-based distance determination. The consortium was subsequently renewed for the development of a new research project, GeoMetre [2], aimed at improving the traceability of geodetic references to the SI meter definition for lengths up to 5 km, which included the development of novel distance meters and a novel strategy for GNSS-based distance determination. This new strategy crystallized in the *Good practice guide on high-accuracy GNSS-based distance metrology* [5], currently in the process of being adopted as Technical Guide by EURAMET, where all relevant error sources are simply characterized along with their uncertainties at the zero differences level and then rigorously propagated to the final baseline length through the particular double-differenced equations used in the estimation. The methodology has been applied to the CERN geodetic network as presented next.

OBSERVATION CAMPAIGN

A subset of five pillars from the CERN geodetic network was selected for the campaign observed by GNSS techniques within the GeoMetre project. Specifically, the pillars selected were those numbered 215 (on top of one of the buildings at CERN Meyrin site), 228, 231, 233 and 353, Fig. 1.

*Corresponding author, serbamo@cgf.upv.es

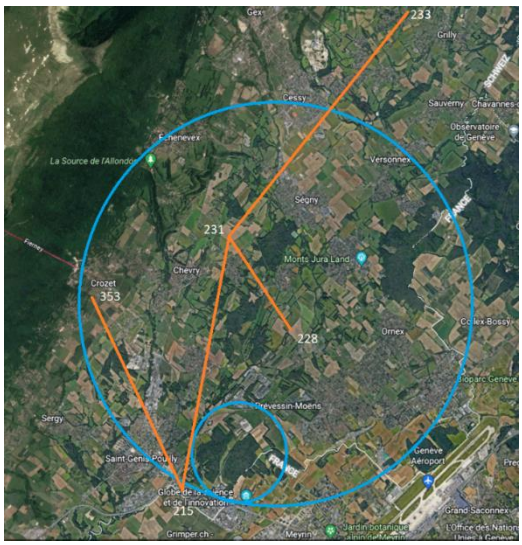

Figure 1: Selected pillars for baseline length determination.

UPV, IGN and CERN jointly carried out the GNSS observation campaign from July 11, 2022, 9:57 GMT to July 14, 2022, 19:05 GMT enabling between 2 days 22.5 hours and 3 days 3 hours of data for the different GNSS stations although a missing data gap of 8 hours at the beginning of July 14 was later discovered for station 233. Five LEICA GR25 GNSS receivers were used along with five individually calibrated LEICA AR25 choke ring antennas to observe the satellites of the four global constellations (GPS, Galileo, GLONASS and BeiDou) with a sampling rate of 1 s. The antenna height on each pillar was accurately measured by IGN using a total station and the same procedure as with the Arpent ADM prototype the week before when measuring the same distances 228-231, 215-353, 215-231 and 231-233. We restrict this presentation to the GBDM+ approach and its comparison with the measurements performed by Kern Mekometer EDM also in the same observing epoch, as well as the comparison with previous values available in the CERN database.

GNSS APPROACH TO LENGTH METROLOGY

The current GNSS approach to length metrology stems from previous works of the group [6-9], which crystallized in the GBDM+ methodology described in the good practice guide [5]. This GBDM+ methodology estimates not only the baseline distance but the contribution of each error source to the distance and the corresponding total uncertainty, which enables using the methodology for metrological purposes.

The minimum equipment for the determination of a baseline length consists of two receivers and two individually calibrated choke ring antennas, along with the necessary auxiliary equipment. The use of identical antenna types (oriented to the North) and identical mountings at both baseline ends is strongly recommended. Determination of antenna heights with folding rules is insufficient, they must be determined by accurate surveying methods (e.g. using a precise total station and reflector). A minimum of 24 h of observed data is recommended so that the residual periodic effects can be averaged out, or, preferably, several days (say three).

With the observed data, a PPP processing is initially carried out for both receivers to obtain information on the error sources and their uncertainties in the receiver-to-satellite line of sight (zero differences). Although one could obtain this initial information from different software – from scientific packages like Bernese to commercial solutions or user-developed software– the use of the online free CSRS-PPP service [10] is proposed as an accurate, simple and friendly solution to obtain a set of initial information both internally consistent and consistent with standard IGS products. The following lists summarize the necessary data to start the GBDM+ baseline length computation.

Initial data:

- GNSS observation files (RINEX format)
- Precise satellite ephemerides and clocks files (SP3 format, obtained from IGS)
- Satellite antenna phase center offsets and variations (ANTEX format, obtained from IGS)
- Individual antenna calibrations (at least by one method) for each of the antennas in use (ANTEX format)

Available data after the initial PPP processing for each station:

- Earth-Centered Earth-Fixed (ECEF) approximate coordinates
- Receiver clock offsets
- Tropospheric delays
- Carrier phase residuals

Functional model

Following [5] we can write the double-differenced carrier phase equation for a pair of receivers i and j and a pair of satellites k and l as

$$\left(\lambda\varphi_{ij}^{kl} - \rho_{ij0}^{kl} - \lambda N_{ij}^{kl} + I_{ij}^{kl} - T_{ij}^{kl} - MP_{ij}^{kl}\right) - \varepsilon_{ij}^{kl} = \left(\frac{\partial\rho_{ij}^{kl}}{\partial X_j}\right)_0 dX_j + \left(\frac{\partial\rho_{ij}^{kl}}{\partial Y_j}\right)_0 dY_j + \left(\frac{\partial\rho_{ij}^{kl}}{\partial Z_j}\right)_0 dZ_j \quad (1)$$

where the double-differenced carrier phase value in cycles φ_{ij}^{kl} for the wavelength λ has been subtracted the approximate double-differenced range ρ_{ij0}^{kl} (computed from the approximated coordinates) and the double-differenced integer ambiguity N_{ij}^{kl}, and corrected with the values of the double-differenced tropospheric delay T_{ij}^{kl} and the double differenced multipath MP_{ij}^{kl}. This multipath can be estimated by sidereal filtering. For the moment, the double-differenced ionospheric delay I_{ij}^{kl} (hopefully given to the public in the next CSRS-PPP release) can be neglected, estimated by applying the Klobuchar model or, in the case of using an iono-free combination, considered as zero.

The three unknowns in Eq. (1), that is the corrections dX_j, dY_j and dZ_j to the approximate coordinates of receiver j (having held fixed receiver i), are multiplied by coefficients which are the corresponding derivatives of the double-differenced range, $\left(\frac{\partial \rho_{ij}^{kl}}{\partial X_j}\right)_0$, $\left(\frac{\partial \rho_{ij}^{kl}}{\partial X_j}\right)_0$ and $\left(\frac{\partial \rho_{ij}^{kl}}{\partial X_j}\right)_0$, respectively. They can be obtained after a least squares adjustment of the system of equations along with the residual ε_{ij}^{kl}. With equations of the type of Eq. (1) we can form the system of equations

$$\boldsymbol{k} + \boldsymbol{r} = \boldsymbol{A}\boldsymbol{x} \tag{2}$$

In the GBDM+ the system of equations Eq. (2) is transformed by using a Jacobian and a rotation matrix to

$$\boldsymbol{k} + \boldsymbol{r} = \boldsymbol{A}\boldsymbol{R}\boldsymbol{J}^{-1}\boldsymbol{x}' \tag{3}$$

so that its solution vector $\boldsymbol{x}'$ directly yields in its first element the corresponding correction to the approximate baseline distance

$$\boldsymbol{x}' = \begin{pmatrix} dD_{ij} \\ d\alpha_{ij} \\ dz_{ij} \end{pmatrix} \tag{4}$$

and the corresponding uncertainty can be obtained in the first element of the covariance matrix.

Error and uncertainty estimation

After double-differencing most of the errors remaining at the zero-differenced level can be assumed to have been completely cancelled (or with completely negligible effects for all practical purposes). For some errors, however, this cannot be safely assumed. It is the case of the double-differenced tropospheric delay, multipath effect and antenna calibration. Their corresponding uncertainties need to be propagated to the double-differenced equations, first, and then through the least squares equations to the final baseline distance. Further details, including the mathematical expressions for uncertainty estimation and propagation are given in [5]. We now show in Figs. 2-4 some results obtained for the current case study.

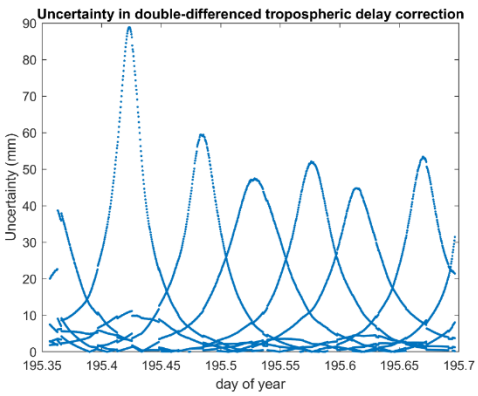

Figure 2: Uncertainty (k = 2) in the double-differenced tropospheric correction for baseline 231-228 and a particular observation period of 8 hours.

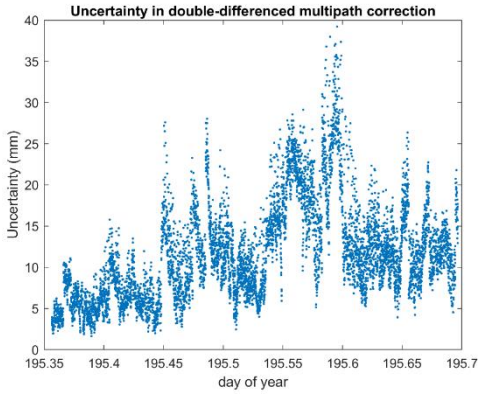

Figure 3: Uncertainty (k = 2) in the double-differenced multipath correction for baseline 231-228 and a particular observation period of 8 h.

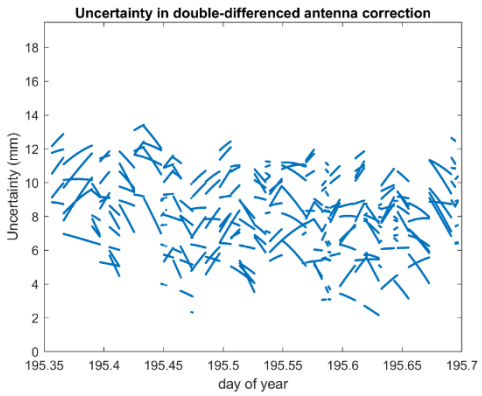

Figure 4: Uncertainty (k = 2) in the double-differenced antenna model correction for baseline 231-228 and a particular observation period of 8 h.

As it can be seen, in this baseline – 231 to 228 – where the height difference is around -55 m, the main uncertainty propagated to double-difference equations, reaching up to several centimetres, comes from the tropospheric delay.

These different uncertainties give rise to the final uncertainty budget as explained in the following subsection.

Uncertainty propagation

The equations to propagate uncertainties in the double-difference equations to the final baseline distance are given in the good practice guide [5]. They include the propagation of double-differenced tropospheric, multipath and antenna model corrections as well as the propagation of the uncertainty by with the antenna height has been determined for each station. In the current case, where the IGN has accurately determined antenna heights by means of a precise total station, we assume the uncertainty in each antenna height to be 0.1 mm. Table 1 shows the uncertainty budget for the baseline distance 231-228, where as in [6]

we have decided to split all the entire GNSS data timespan available in different time blocks of different lengths up to 8 hours for obtaining different solutions whose consistency can be analyzed (see the following subsection). The uncertainty in the baseline distance due to the uncertainty in antenna heights is given as zero since the value obtained after uncertainty propagation is below one hundredth of a millimeter (0.000007 m). Also negligible was considered the effect of monument instability during the measurements.

Table 1: Total uncertainty budget in the baseline distance 231-228 propagated from all relevant error sources, values in mm (average values for each of the different time blocks), k = 2.

Obs. time span (h)	$u_{\text{tropo.delay}}$	$u_{\text{multipath}}$	$u_{\text{ant.cal.}}$	u_{total}
1	1.79	0.86	0.90	2.24
2	1.21	0.58	0.61	1.50
3	0.95	0.46	0.48	1.18
4	0.84	0.41	0.42	1.04
6	0.67	0.34	0.34	0.83
8	0.58	0.30	0.29	0.72

Baseline lengths

In Fig. 5 we can see the values obtained for baseline 231-228 for each of the different time computation blocks. The variation between the different solutions is less than 1 mm and agrees completely with the observed dispersion. The weighted average value gives a final value for the distance of 2235.6911 m.

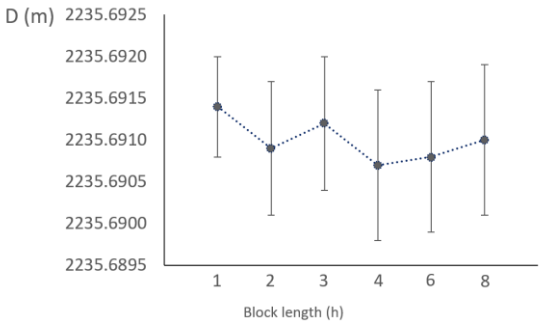

Figure 5: Baseline distance 231-228, values in m. The average values for each of the different time blocks are indicated with the blue dots and the typical dispersion (k = 2) with the error bars.

In Fig. 6 we can see the values obtained for baseline 215-353 for each of the different time computation blocks. The variation between the different solutions is below 1 mm and agrees with the observed dispersion except for the two first time blocks that locate significantly apart. This might be an undesired effect of random nature or, as experienced in [6], it could be that due to the short timespan there were systematic errors not fully compensated that affect the result obtained for the distance. The weighted average value gives a final value for the distance of 4753.1237 m.

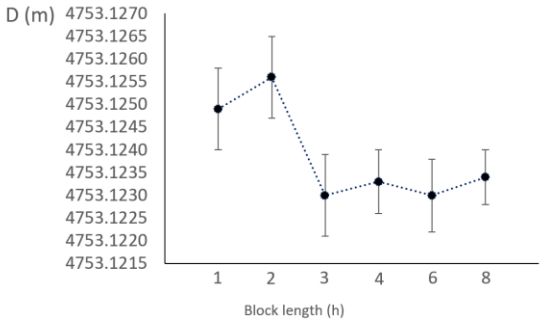

Figure 6: Baseline distance 215-353, values in m. The average values for each of the different time blocks are indicated with the blue dots and the typical dispersion (k = 2) with the error bars.

In Fig. 7 we see the values for baseline 231-215. The dispersion of the solutions with shorter computation blocks, especially for the one hour timespan, is unexpectedly high. However, the variation between the different solutions does agree well with the observed dispersion. The weighted average value gives a final value for the distance of 6019.4459 m.

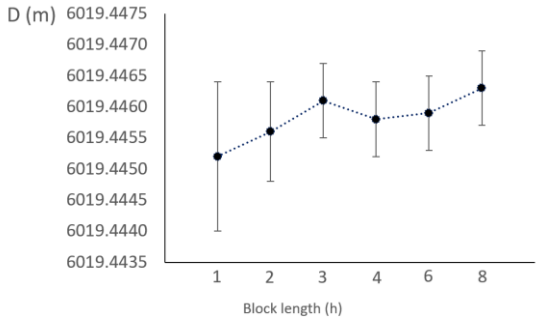

Figure 7: Baseline distance 231-215, values in m. The average values for each of the different time blocks are indicated with the blue dots and the typical dispersion (k = 2) with the error bars.

In Fig. 8 we see the values for baseline 233-231. They agree well between the different solutions as well as with the observed dispersion. The weighted average value gives a final value for the distance of 6542.0130 m.

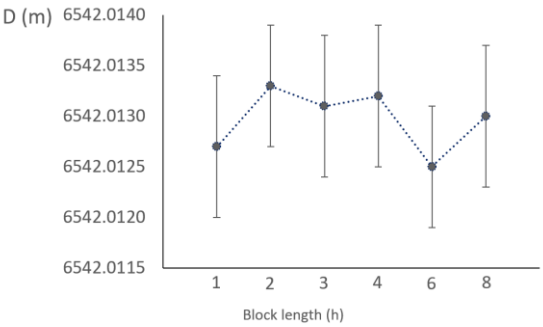

Figure 8: Baseline distance 233-231, values in m. The average values for each of the different time blocks are indicated with the blue dots and the typical dispersion (k = 2) with the error bars.

In Table 2 we give a summary of baseline distances and corresponding uncertainties, taking these as the average values for the 8-hour time blocks.

Table 2: Baseline distances and uncertainties, values in m, k = 2.

Baseline	Distance	u_{total}
231-228	2235.6911	0.0007
215-353	4753.1237	0.0006
231-215	6019.4459	0.0008
233-231	6542.0130	0.0008

COMPARISON WITH KERN MEKOMETER ME5000

The CERN Mekometer ME5000 with serial number 357034 was used along with UPV meteorological sensors to measure the distance of the baselines with clean direct intervisibility: baselines 231-228 and 215-353. The instrument had its frequency calibrated at the UPV calibration laboratory, resulting in a virtually zero scale correction (-0.030 ± 0.015 ppm, k = 2). After applying meteorological corrections and reduction to the pillar height references the resulting distances along with the experimental deviations where 2235.6934 ± 0.0013 m (k = 2) for the baseline 231-228 and 4753.1223 ± 0.0017 m (k = 2) for the baseline 215-353. The values of these experimental deviations agree well with those expected from the nominal uncertainty of the EDM along with the respective uncertainties in meterorological parameters.

The comparison with the values derived from the GBDM+ method yields a difference of -0.0023 m for the baseline 231-228 and 0.0014 m for baseline 215-353. This is a good agreement, the second value being well inside the combined uncertainty limit and the first just above the limit for k =2, especially considering the existing limiting factors: first, the refraction correction for the EDM distances was determined by using parameters measured only at the ends of each baseline, which is only considered reliable for distances less than 1 km; second, the EDM reflector was not calibrated and its offset was considered to be exactly zero, the CO_2 content in Geneva at the time of the measurements was taken as the worldwide average in July (421 ppm), etc.

COMPARISON WITH OTHER CAMPAIGNS AT CERN

CERN has a long record of observations of their geodetic network. They have been made with different instruments, computing software and, unfortunately, sometimes referred to different or unclear altimetric references in the pillars, which add up to the possible long-time instability of the monuments, which can reach up to several mm [11]. We analyse here three distances that have a long observation record and compare their different values available with the determinations by GBDM+ and ME5000 in the 2022 campaign. The results can be shown in Fig. 9, where the different y axes in the subplots have been shown with the same scale for a better comparison.

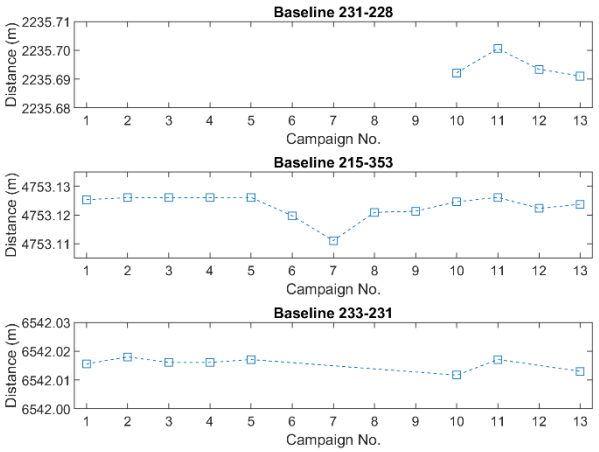

Figure 9: Baseline distances 231-228, 215-353 and 233-231 for different campaigns or registry times: 1 CCS86, 2 CCS98, 3 CCS2000, 4 CCS2001, 5 Geode2006, 6 Mekometer-2017, 7 TCRP1201-2017, 8 Bernese-2017, 9 GravNet-2017, 10 IGN-2017, 11 Geode2022, 12 GeoMetre_Mekometer-2022, 13 GeoMetre_GBDM+-2022.

Apart from one value in the database that has not been depicted –the case of the distance 231-228 in Geode database 2006, which is some 30 cm larger than the rest of the values for this distance– the different determinations of the different distances agree among them within 1 or 2 cm.

CONCLUSIONS, LIMITATIONS AND FUTURE WORK

The four baselines selected from the CERN geodetic network and continuously observed during 3 days have been processed by the GBDM+ approach without significant problems (despite the 8-hour data gap discovered in one station). The distance and corresponding uncertainty budget were obtained for each of the baselines. A few large dispersions and slight inconsistencies between the different results obtained for the 215-353 as well as the 231-215 baselines were experienced, within an otherwise overall satisfactory solution for the case study.

Some limitations still exist, namely:

- In its current version (version 3), the CSRS-PPP service estimates ionospheric delays but does not distribute them to the users. The CSRS-PPP may possibly add this output in short as part of its forthcoming version 4 (Banville 2021, personal

communication). For the moment, the double-differenced ionospheric effect has been considered completely negligible with no uncertainty included in the uncertainty budget.

- In its current version (version 3), the CSRS-PPP service truncates all input files to a sampling rate of 30 s, so that no corrections and corresponding uncertainty values are available for shorter rates. This prevents a complete analysis of uncertainty at sampling rates shorter than 30 s, which is the sampling rate we have therefore selected for the current solution.
- The sidereal filtering approach to determine a multipath model that provides a correction value along with an uncertainty is only possible for the GPS constellation due to the corresponding repeat periods of the different GNSS constellations. This prevents a complete analysis of uncertainty for satellites from constellations other than GPS, which is the only we have used for the current solution.
- The possibility of eliminating double-difference equations with large uncertainties, or better yet, those whose uncertainties have a large impact on the resulting distance, as well as the resulting degree of improvement, still remains unexplored.

The comparison with the distances obtained with the Kern Mekometer ME5000 provides results fairly consistent with the ones shown in the present report, thus confirming their validity.

ACKNOWLEDGMENT

The work leading to this paper was performed within the 18SIB01 GeoMetre project of the European Metrology Programme for Innovation and Research (EMPIR). This project has received funding from the EMPIR programme co-financed by the Participating States and from the European Union's Horizon 2020 research and innovation programme, funder ID: 10.13039/100014132. Raquel Luján acknowledges funding from the Programa de Ayudas de Investigación y Desarrollo (PAID-01-20) de la Universitat Politècnica de València. We are also grateful to José María Grima for his support to calibrate the frequency of the Kern Mekometer ME5000 at the UPV Calibration Laboratory.

REFERENCES

[1] G.R. Huggett, Two-color terrameter, Tectonophysics, 71 (1981), 29-39, https://doi.org/10.1016/0040-1951(81)90044-5.

[2] F. Pollinger, S. Baselga, C. Courde, C. Eschelbach, L. García-Asenjo, P. Garrigues, J. Guillory, P.O. Hedekvist, T. Helojärvi, U. Kallio, T. Klügel, P. Köchert, M. Lösler, R. Luján, T. Meyer, P. Neyezhmakov, D. Pesce, M. Pisani, M. Poutanen, G. Prellinger, A. Röse, J. Seppä, D. Truong, R. Underwood, K. Wezka, J.P. Wallerand and M. Wiśniewski, "The European GeoMetre project – developing enhanced large-scale dimensional metrology for geodesy," 5th Joint International Symposium on Deformation Monitoring (JISDM), Valencia, June 20-22, 2022; https://jisdm2022.webs.upv.es.

[3] F. Pollinger, A. Bauch, J. Leute, K. Meiners-Hagen, J. Mildner, J. Guillory, J.-P. Wallerand, J. Jokela, U. Kallio, H. Koivula, S. Lahtinen, M. Poutanen, M. Astrua, C. Francese, M. Zucco, L. Eusebio, F. Marques, C. Pires, F. Saraiva, O. Pellegrino, T. Tomberg, T. Hieta, T. Fordell, M. Merimaa, V. Kupko, P. Neyezhmakov, S. Bergstrand, S.A. van den Berg, T. Kersten, T. Krawinkel, S. Schön, C. Homann, D. Tengen, W. Niemeier, B. Görres, F. Zimmermann, H. Kuhlmann, N. Bhattacharya, A. Lesundak and A. Bosnjakovic, "JRP SIB60 Metrology for Long Distance Surveying- a concise survey on major project," 3rd Joint International Symposium on Deformation Monitoring (JISDM), Vienna, March 30–April 1, 2016; https://www.fig.net/resources/proceedings/2016/2016_03_jisdm_pdf/nonreviewed/JISDM_2016_submission_16.pdf

[4] A. Bauch, L. Eusébio, U. Kallio, H. Koivula, H. Kuhlmann, S. Lahtinen, F. Marques, O. Pellegrino, C. Pires, F. Pollinger, M. Poutanen, F. Saraiva, S. Schön and F. Zimmermann, *Good practice guide for high accuracy global navigation satellite system based distance metrology. Revised Version 2* (Braunschweig: JRP SIB60 Surveying Consortium, 2017).

[5] S. Baselga, L. García-Asenjo, P. Garrigues, R. Luján, F. Pollinger, U. Kallio, H. Koivula, K. Wezka, D. Próchniewicz, D. Pesce and S. Bergstrand, *Good practice guide on high-accuracy GNSS-based distance metrology*. (EURAMET Technical Guide, in preparation, 2022).

[6] S. Baselga, L. García-Asenjo and P. Garrigues, "Submillimetric GPS distance measurement over short baselines: case study in inner consistency" Meas. Sci. Technol. 24 (2013) 075001, 8 pp. https://doi.org/10.1088/0957-0233/24/7/075001

[7] S. Baselga, L. García-Asenjo and P. Garrigues, "Submillimetric GPS distance measurement over short baselines: noise mitigation by global robust estimation" Meas. Sci. Technol. 25 (2014) 105004, 6 pp. http://doi.org/10.1088/0957-0233/25/10/105004

[8] L. García-Asenjo, S. Baselga, C. Atkins and P. Garrigues, "Development of a Submillimetric GNSS-Based Distance Meter for Length Metrology", Sensors, 21 (2021) 1145, 21 pp. https://doi.org/10.3390/s21041145

[9] S. Baselga, L. García-Asenjo, P. Garrigues, and R. Luján, "GBDM+: An improved methodology for a GNSS-Based Distance Meter", Meas. Sci. Technol. 33 (2022), 085020, 16 pp. https://doi.org/10.1088/1361-6501/ac6f45

[10] S. Banville, E. Hassen, P. Lamothe, J. Farinaccio, B. Donahue, Y. Mireault, M.A. Goudarzi, P. Collins, R. Ghoddousi-Fard and O. Kamali, "Enabling ambiguity resolution in CSRS-PPP" Navigation 68 (2021) 433–51. https://doi.org/10.1002/navi.423

[11] R. Haas, S. Bergstrand and W Lehner, "Evaluation of GNSS Monument Stability". In: Altamimi, Z., Collilieux, X. (eds) Reference Frames for Applications in Geosciences. International Association of Geodesy Symposia, vol 138. (Heidelberg: Springer, 2013). https://doi.org/10.1007/978-3-642-32998-2_8